



Numerical Study on Subsurface Stress in Hertzian Contacts under Pure Sliding Conditions

Fadi Ali¹

Faculty of Technical Engineering, Tartous University, Tartous, Syria, Email: fadieskanderali@gmail.com

Received October 24 2019; Revised December 28 2019; Accepted for publication December 29 2019.

Corresponding author: Fadi Ali (fadieskanderali@gmail.com)

© 2020 Published by Shahid Chamran University of Ahvaz

Abstract. In this study, the two-dimensional numerical simulation on the subsurface stress field in Hertzian contact under the pure sliding condition for different speeds and coefficients of friction is presented. The Hertzian contacts are represented by a dry contact between a rigid flat surface and an elastic cylinder with radius $R=12.5$ mm. Simulation is carried out through two steps, the first one is for applying normal load and the second one is for applying angular speed for the cylinder. The results of subsurface stress filed for pure sliding are compared to non-moving Hertzian contact. The results show that pure sliding speed has a major effect on the value of maximum von Mises stress in the subsurface of contact. The effect of sliding speed is attributed to tangential forces and elastic deformation in the contact. On the other hand, the coefficient of friction has a primary effect on the position of maximum stress and the shift of the contact region. Indeed, when pure sliding motion is introduced with a low value of friction coefficient, the shift of the contact region is negligible compared to non-moving Hertzian contact. The study is extended to investigate the effect of contact geometry on subsurface stress for Hertzian contact in the cam-follower interface. The shape of the follower has a significant effect on the value and distribution of Hertzian stress, thus, the fatigue life of rubbing surfaces of the cam-follower interface.

Keywords: Sliding speed; Friction; Finite element analysis; Von Mises stress; Cam-follower.

1. Introduction

Mechanical interfaces with Hertzian contacts subjected to repeated rolling and sliding load are common in industrial and engineering applications. The plastic deformation and subsurface stress concentration under the action of repeated loading likely lead to fatigue failure over time. Usually, rolling and sliding concentrated contacts (point or line contacts) such as in rolling-elements bearings, cams, and gears, are lubricated to reduce friction, nevertheless, the stress is still subjected to Hertzian theory [1,2,3], where the pressure can reach extremely high values in the scale of gigapascal. Introducing the sliding motion to surfaces with Hertzian contact increases the severity of operating conditions due to friction and tangential traction forces. In Hertzian contacts, either lubricated or dry, high stress is localized in a very small volume of material because the contact dimensions are usually limited in the scale of 200-1000 μm [4].

Hertzian contact problem under rolling/sliding motion has been studied by many researchers. Hamilton and Goodman [5] studied the complete stress field created by a circular sliding contact subjected to a hemispherical Hertzian normal pressure with emphasis on the effect of friction. They revealed that the increase of friction results in moving the region of the maximum yield stress towards the surface. Similarly, Bryant and Keer [6] investigated the surface and subsurface stresses and displacements for elliptical rough contact between two identical curved bodies. The results show that tangential tractions along the minor axis of the elliptical contact have a larger maximal tensile stress compared to the tangential tractions oriented along the major axis. Chen [7] studied the deformations of two elastic bodies with contact for anisotropic materials under indentation with and without sliding. The results show that the maximum shear



stress is located in the vicinity of the contact area in the anisotropic indentation. A simplified micro-macro contact model is presented by Zhou and Cheng [8] for rolling and sliding contact to calculate pressure distribution and subsurface stress created by asperity to asperity contacts. The pressures related to asperity interaction and the subsurface stress map have been analyzed by superimposing the asperity contacting loads on the Hertzian load. A contact model has been developed by Chen et al [9, 10] for steady-state and transient contact heat transfer with the effect of sliding speed and thermal softening. They demonstrated that the temperature and contact pressure increase with increasing the sliding speed. Lee and Ning Ren [11] presented a three-dimensional numerical simulation on the subsurface stress field for rough surfaces in sliding contact with traction. The simulation is carried out for two values of friction coefficients, i.e., $f=0.00$ and $f= 0.25$. In both cases, the rough surface has higher stress compared to the smooth surface. Similar results are presented by Bailey and Sayles [12] on the effects of sliding friction on stresses in non-conformal contact of rough bodies. They investigated high stress on the surface due to the roughness. More recently, Zhang et al [13] showed by means of numerical simulation that the maximum von Mises stress in the substrate increases with the increase of friction coefficient and the profile of normal pressure near the end of the contact is shifted towards the trailing edge due to tangential effects. The tribological behavior of lubricated textured Hertzian contacts under rolling/sliding motion is profoundly studied numerically and experimentally in [14, 15, 16].

Indeed, Hertzian contact analysis is deeply clarified in the literature under steady-state and mixed rolling/sliding conditions [17-20]. However, relatively little work concerning the behavior of Hertzian contacts under pure sliding (one surface is stationary) conditions has been reported. Pure sliding of mechanical assemblies with Hertzian contact is common and it can be divided into two types: - transitional pure sliding (such as in the piston ring and cylinder liner assembly, hydraulic Seals, Gaskets, and O-rings) - rotational pure sliding (such as in cam and flat-faced follower, some human joints). The present paper provides a numerical simulation on the subsurface stress in Hertzian contacts under pure sliding conditions.

2. Theoretical Background

2.1 Hertzian contact of rigid flat surface and elastic curvature

The contact of two parallel cylindrical bodies is considered as a Hertzian line contact. In this case, the half-width of the contact (a) and the maximum contact pressure (P_H) are given by [3] as the following:

$$a = \left(\frac{4WR}{\pi E^*} \right)^{1/2}, \quad P_H = \left(\frac{WE^*}{\pi R} \right)^{1/2}, \quad \frac{1}{E^*} = \frac{1-\nu_1^2}{E_1} + \frac{1-\nu_2^2}{E_2}, \quad \frac{1}{R} = \frac{1}{R_1} + \frac{1}{R_2} \tag{1}$$

where W is the normal applied load per unit length, E^* is the equivalent Young's modulus, E_1, E_2 and ν_1, ν_2 are Young's moduli and Poisson's ratios for the lower and upper body in contact respectively, R is the equivalent radius of curvature, R_1, R_2 are the radii of curvature of the lower and upper body in contact respectively. For the rigid flat surface, $E_2=\infty$ and $R_2=\infty$. The distribution of contact pressure is given as the following:

$$P(x) = P_H \sqrt{1 - \left(\frac{x}{a} \right)^2} \tag{2}$$

where x is a radial coordinate measured from the center of the contact.

2.2 Subsurface stress of contact

For Hertz line contact in steady-state, the magnitude of the plane stress (xz plane) components below the surface as a function of the maximum pressure of contacting bodies is given by [21] as the following:

$$\sigma_x = - \frac{P_H}{(1 + \zeta^2)^{1/2}} \left[2\zeta^2 + 1 - 2\zeta(1 + \zeta^2)^{1/2} \right] \tag{3}$$

$$\sigma_z = - \frac{P_H}{(1 + \zeta^2)^{1/2}} \tag{4}$$

where $\zeta = z/a$ is a nondimensional parameter. Then the subsurface shear stress is given as:

$$\tau_{xz} = ((\sigma_x - \sigma_z)/2) \tag{5}$$

The resulting equivalent von Mises stress can be written as:

$$\sigma_{vMises} = \sqrt{3} \tau \tag{6}$$

where τ is shear stress.



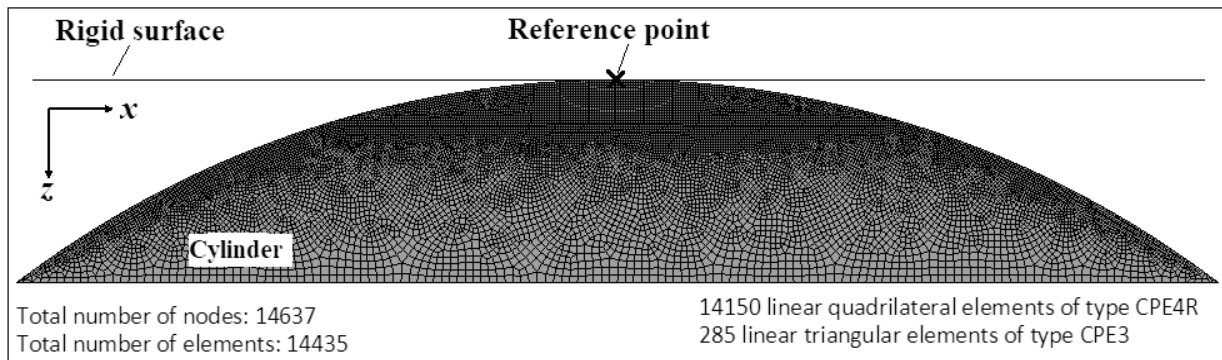


Fig. 1. The mesh used for contact simulation

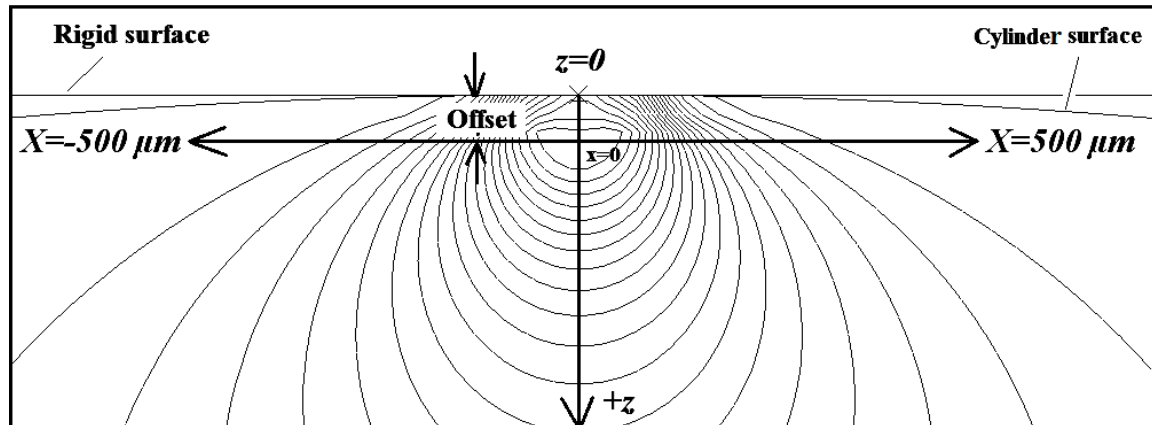


Fig. 2. Coordinate system for capturing the values of subsurface stress.

3. Numerical Simulation Procedure

3.1 Finite-element analysis (FEA)

Commercial finite-element analysis package (ABAQUS/Explicit) is used to simulate the two-dimensional subsurface stresses in the sliding contact between a rigid flat surface and a perfectly elastic cylinder under the assumption of plane strain behavior. Effects of adhesion, stick-slip and sliding-generated heat are not taken into the account in the present study. The interaction between surfaces is defined with the finite-sliding and surface-to-surface formulation. The configuration of the contact is set as shown in Fig. 1. The reference point on the rigid surface has constraints for rotation and motion in the direction of the x-axis. The radius of the cylinder is $R_I = 12.5 \text{ mm}$. The displacement of a rigid surface is set to $\delta = 2.5 \mu\text{m}$ on the z-axis in the first step of a simulation. The displacement δ is corresponding to the normal load per unit length $W' = 343 \text{ kN/m}$. The cylinder is coupled to a constrained reference point in its center. Cylinder has constraints for motion in the direction of the x-axis and z-axis. In the second step of simulation, pure sliding between the rigid surface and cylinder is achieved by giving a constant angular speed (ω) to the cylinder around its reference point localized in the center. Hence, the linear sliding speed is calculated as $U_{\text{cylinder}} = R \cdot \omega$. The simulation is carried out under different frictional pure sliding conditions for low velocities in general to avoid the effects of heat generation in the contact. The contact is subjected to the tangential behavior of the penalty contact method. Material properties used in simulation: Elastic modulus (E) (GPa) 210, Poisson's ratio (ν) 0.3, Yield stress (MPa) 450, Density (ρ) 7810 kg/m^3 . The segment of the cylinder shown in Fig. 1 is meshed using a four-node plane strain element CPE4R. In order to reduce errors, a finer mesh is used in the vicinity of the contact as shown in Fig. 1. The total number of nodes is 14637, the total number of elements is 14435. 14150 linear quadrilateral elements are of type CPE4R, 285 linear triangular elements are of type CPE3.

3.2 Coordinate system

Fig. 2 shows the coordinate system for capturing the values of subsurface stress. The stress is captured along the axis of symmetry (z-z axis). z-z axis starts from the surface of the cylinder where $z=0$ to the value of $z=2000 \mu\text{m}$. The offset between the flat deformed surface where $z=0$ and x-x axis, is set at the depth where the peak value of the subsurface stress is localized on the z-z axis. Von Mises stress on x-x is shown for distance from $x=-500 \mu\text{m}$ to $x=+500 \mu\text{m}$. the position of $x=0$ is localized in the middle of this distance.



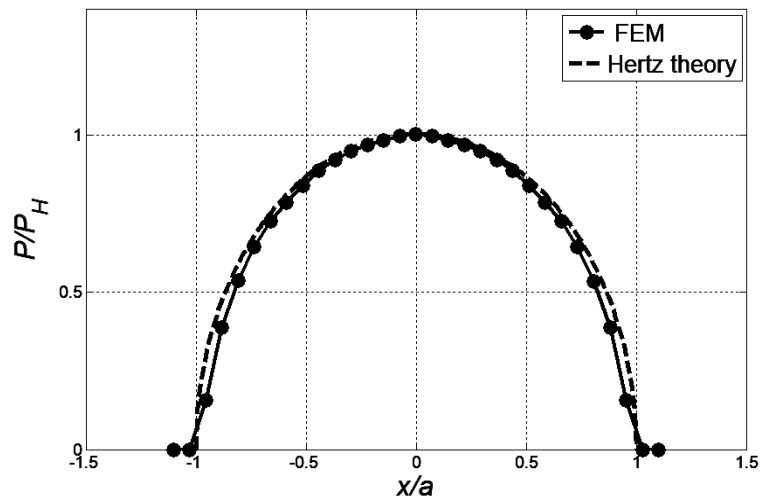


Fig. 3. Comparison of normalized Hertzian pressure (P/P_H) distribution along x-axis based on theory and FE model.

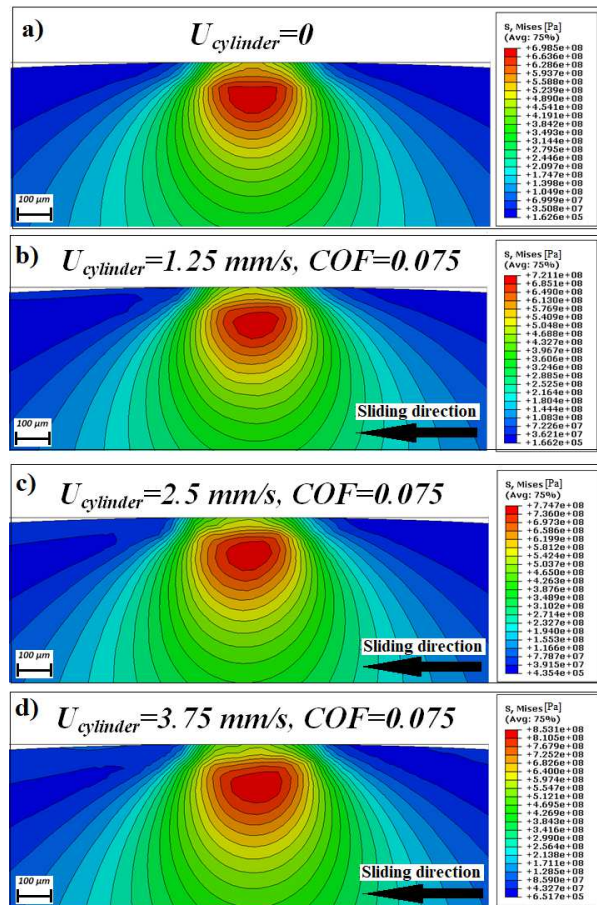


Fig. 4. Effect of sliding speed on von Mises subsurface stress distribution in Hertzian contact for $COF=0.075$, a) $U_{cylinder}=0$, b) Pure sliding, $U_{cylinder} = 1.25 \text{ mm/s}$, c) Pure sliding, $U_{cylinder} = 2.5 \text{ mm/s}$, d) Pure sliding, $U_{cylinder} = 3.75 \text{ mm/s}$.

3.3 Verification of FE model

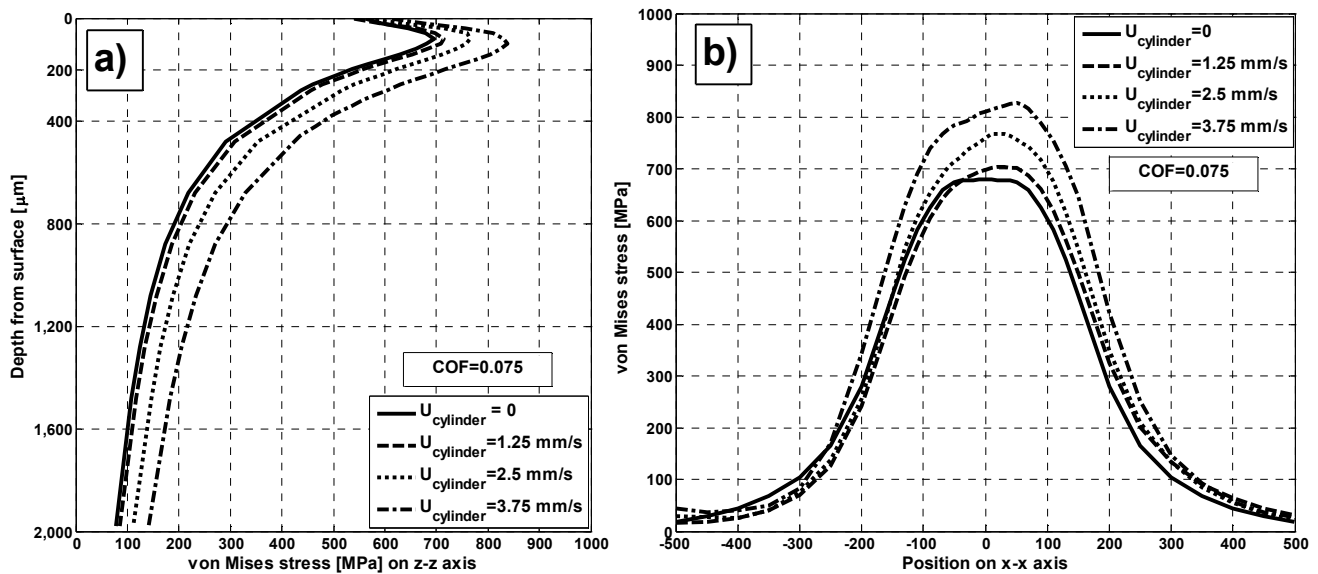
Table 1 shows a comparison of basic values of maximum Hertzian pressure P_H , maximum shear stress τ_{max} (MPa) and contact half-width a for FE model and classical Hertzian theory. In general, the variation is limited and there is a good correlation between the results. The variation between theory and finite element analysis (FEA) in Table 1 depends on the number, type, and distribution of meshing elements and the process of mesh refining. However, a reasonable computational time is required for accepted accuracy. Also, the applied contact constraints and the method of applying load during the steps of simulation have an effect on the accuracy of results.

Fig. 3 depicts the normalized pressure distribution (P/P_H) in the contact based on the Hertzian theory and FE model. Again, good consistency is obtained for the pressure profile from the FE model.



Table 1. Comparison of values for FE model and Hertzian theory.

	Theory	FEA	Variation
Maximum Hertzian pressure P_H (GPa)	1.42	1.38	2.8%
Maximum shear stress τ_{max} (MPa)	$0.3P_H=426$	403	5.4%
Contact half width a (μm)	154	150	2.6%
Depth of maximum shear stress z (μm)	$0.78a=120$	112	6.7%

**Fig. 5.** Effect of sliding speed on subsurface stress in Hertzian contact for $COF=0.075$ along, a) z-z axis, b) x-x axis.

4. Results and Discussion

4.1 Effect of sliding speed

Results in Fig. 4 depict the von Mises subsurface stress contour in Hertzian contact for speeds a) $U_{cylinder}=0$, b) $U_{cylinder}=1.25$ mm/s, c) $U_{cylinder}=2.5$ mm/s, d) $U_{cylinder}=3.75$ mm/s under pure sliding conditions (rigid surface is stationary). In this simulation, a constant coefficient of friction $COF=0.075$ is set for the contact interaction. It is clear from Fig. 4 that the maximum von Mises subsurface stress tends to increase with increasing the sliding speed and the contact region shifts towards the trailing edge in the opposite direction of sliding. This behavior is attributed to the increased effect of tangential traction and deformations in the contact as the sliding speed increases. The subsurface stress field along the z-z and x-x axis is shown in Fig. 5. It is clear from Fig. 5.a that the general profile of subsurface stress distribution along the z-z axis is unchanged for all speeds. However, the peak of maximum von Mises stress along the z-z axis increases with increasing the sliding speed and the position of the stress peak under the surface is nearly the same regardless of the pure sliding speed. The position of von Mises stress peak along the z-z axis is located at a depth of about $112 \mu\text{m}$ for all speeds, this is attributed to very low sliding speeds applied in the simulation where the depth of von Mises stress peak is not affected so much by changing the speed. Fig. 5.b depicts the effect of sliding speed on subsurface stress along the x-x axis at a depth of $112 \mu\text{m}$ under pure sliding for $COF=0.075$. It is evident from Fig. 5.b that the presence of sliding causes a major change and asymmetry in the distribution of subsurface stresses along the x-x axis. As can be seen clearly from Fig. 5.b, the magnitude of maximum von Mises stress increases with increasing sliding speed. The region of maximum von Mises stress is shifted in the direction of the trailing edge of Hertzian contact (the opposite direction of sliding) as the sliding speed increases.

4.2 Effect of coefficient of friction (COF)

Numerical simulation is carried out in this section to investigate the effect of the coefficient of friction (COF) on the subsurface stress field in Hertzian contact under pure sliding conditions. The effect of two values of friction coefficient $COF=0.01$ and $COF=0.15$ are compared under a constant pure sliding speed $U_{cylinder}=2.5$ mm/s as shown in Fig. 6. The results are compared with the subsurface stress field for Hertzian contact when the cylinder is stationary $U_{cylinder}=0$. It is clear from Fig. 6 that increasing the coefficient of friction results in increasing the maximum von Mises stress in the contact. Maximum stress increases from 764.9 MPa to 802.6 MPa when the friction coefficient increases from $COF=0.01$ to $COF=0.15$ for the same sliding speed $U_{cylinder}=2.5$ mm/s. However, Fig. 6 shows that the region of maximum stress is not shifted to the direction of sliding for the low value of $COF=0.01$ while the region of maximum stress is apparently shifted in the direction of sliding for the larger value of $COF=0.15$. Thus, the position of maximum subsurface stress is significantly related to the value of the friction coefficient.



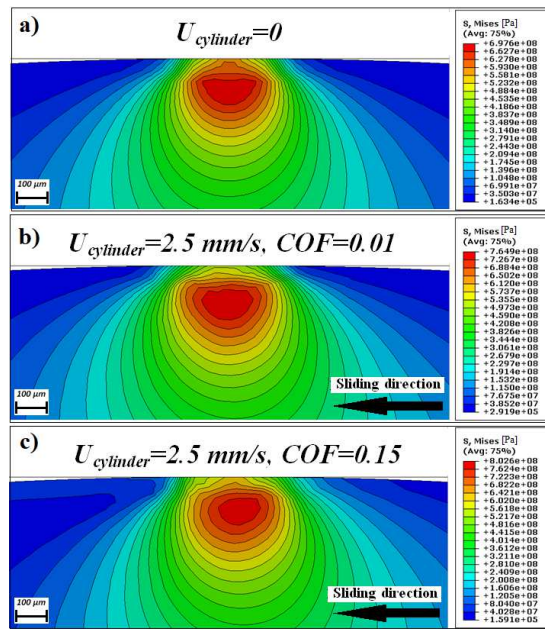


Fig. 6. Effect of friction coefficient value on von Mises stress distribution in Hertzian contact, a) $U_{cylinder}=0$, b) Pure sliding, $U_{cylinder}=2.5$ mm/s, $COF=0.01$, c) Pure sliding, $U_{cylinder}=2.5$ mm/s, $COF=0.15$.

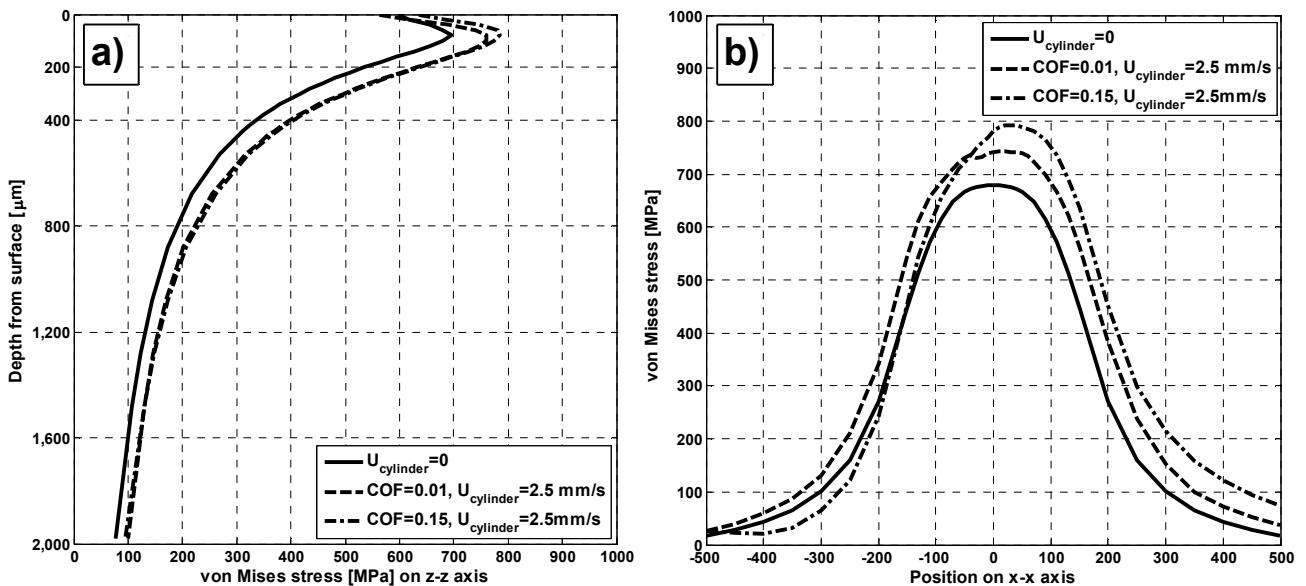


Fig. 7. Effect of the coefficient of friction on subsurface stress in Hertzian contact along, a) z-z axis, b) x-x axis.

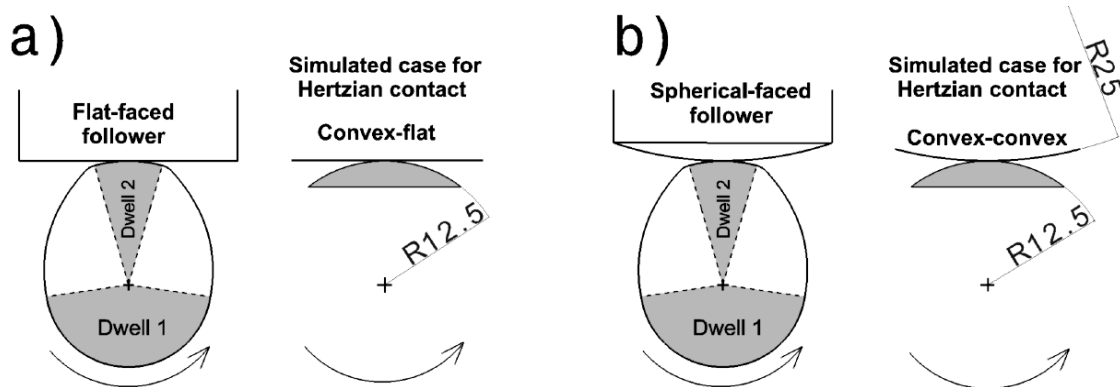


Fig. 8. Schematic representation of Hertzian contact in cam-follower mechanism based on the geometry of follower, a) flat-faced follower, b) spherical-faced follower.



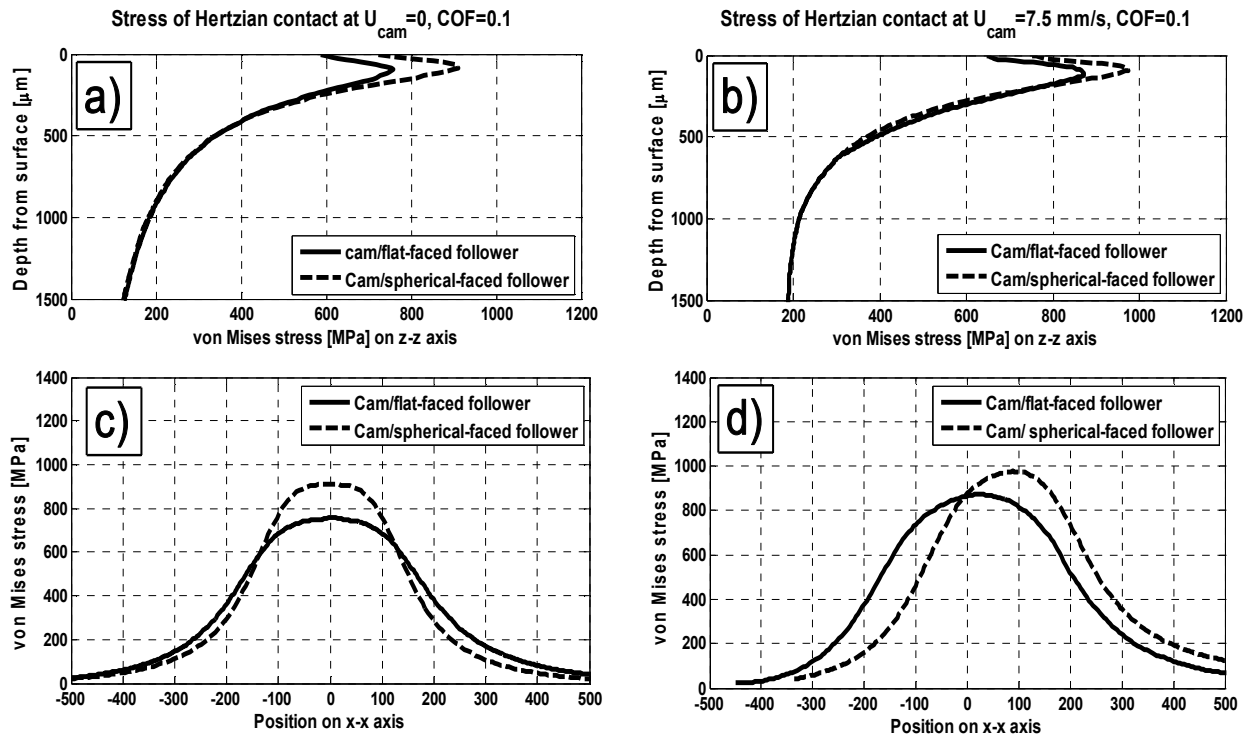


Fig. 9. Effect of of follower geometry on subsurface stress, a) on z-z axis at $U_{cam}=0$, b) on z-z axis at $U_{cam}=7.5 \text{ mm/s}$, c) on x-x axis at $U_{cam}=0$, b) on x-x axis at $U_{cam}=7.5 \text{ mm/s}$.

Fig. 7 shows the distribution of the subsurface stress field along the z-z and x-x axis. From Fig. 7.a, it is evident that introducing the sliding motion leads to the increase of maximum von Mises stress along the z-z axis in the contact compared to the non-moving Hertzian contact. Indeed, Fig. 7.a shows a marginal effect of friction coefficient on the distribution of subsurface stress along the z-z axis and the change is limited to the value of stress peak.

Fig. 7.b shows that even when the sliding speed is introduced in the contact with a small value of friction coefficient $COF=0.01$, there is a negligible effect on shifting the region of maximum stress along the x-x axis compared to non-moving Hertzian contact. In addition, the distribution of stress along the x-x axis for the contact with $COF=0.01$ is approximately symmetrical alike to non-moving contact as shown in Fig. 7.b. However, the region of maximum stress along the x-x axis is significantly shifted to the opposite direction of sliding when sliding speed is introduced in the contact with a large value of friction coefficient $COF=0.15$.

4.3 Effect of follower geometry on subsurface stress in Hertzian contact of cam-follower interface

Cam-follower interfaces are common in many industrial and engineering applications. Fig. 8 shows a schematic representation of Hertzian contact in a cam-follower interface based on the geometry of follower, where a double-dwell cam is in contact with a) flat-faced follower b) spherical-faced follower. Dwell is the angle through which the cam turns while the follower remains stationary at the highest or the lowest point of the lift. Thus, pure sliding motion is pronounced in the Hertzian contact between the cam and follower during the stroke of dwell. In Fig. 8, Dwell 1 represents the pure sliding over the base circle of the cam profile, while Dwell 2 represents the pure sliding over the peak lift region of the cam profile. Usually, the region of peak lift of the cam profile is highly stressed due to the compression of the retaining spring. In the numerical simulation, it is assumed that the follower is rigid and non-rotating. Hertzian contact between the cam and flat-faced follower is represented by a deformable convex surface (radius=12.5 mm) and a rigid flat surface (radius= ∞). In the case of spherical-faced follower, Hertzian contact is represented by a deformable convex surface (radius=12.5 mm) and a rigid convex surface (radius=25 mm). The material of the deformable segment of the cam is considered as steel ($E=210 \text{ GPa}$, $\nu=0.3$). The applied load on cam results from the inertia and spring forces, however, the calculations are carried out for a constant load per unit length of 400 kN/m at the maximum lift position in case a) and b). The speed of the cam surface at the maximum lift is set to $U_{cam}=7.5 \text{ mm/s}$ and the coefficient of friction is set to $COF=0.1$.

Fig. 9 shows the results of numerical simulation for the effect of of follower geometry on subsurface stress, a) on z-z axis at $U_{cam}=0$, b) on z-z axis at $U_{cam}=7.5 \text{ mm/s}$, c) on x-x axis at $U_{cam}=0$, b) on x-x axis at $U_{cam}=7.5 \text{ mm/s}$. Fig. 9.a and Fig. 9.b show that for $U_{cam}=0$ and $U_{cam}=7.5 \text{ mm/s}$, the spherical-faced follower has a larger peak of von Mises stress on the z-z axis compared to flat-faced follower under the same loading. Similar results are depicted in Fig. 9.c and Fig. 9.d for the von Mises stress on the x-x axis.

The maximum von Mises stress for flat-faced follower at $U_{cam}=0$ is 760 MPa corresponding to a displacement of the cam surface of $2.87 \mu\text{m}$ and contact half-width $a=166 \mu\text{m}$, while the maximum von Mises stress for spherical-faced follower at



$U_{cam}=0$ is 908 MPa corresponding to a deformation of the cam surface of 2.98 μm and contact half-width $a=136 \mu\text{m}$. Indeed, the curved surface of spherical-faced follower leads to the larger value of von Mises stress peak on z-z and x-x axes and larger deformation of the cam surface at $U_{cam}=0$. At sliding speed $U_{cam}=7.5 \text{ mm/s}$, the maximum von Mises stress for the flat-faced follower is increased to 881 MPa and for the spherical-faced follower is increased to 979 MPa. As a result, the cam and follower contact are subjected to more severe fatigue conditions when the spherical-faced follower is used. Nevertheless, many researchers [22, 23] ensured that the spherical-faced follower shows an enhanced performance and wear resistance compared to the flat-faced follower. This is attributed to improved lubrication conditions in the contact of the cam and spherical-faced follower. The lubricant film thickness is enhanced at the maximum lift position of the cam as the follower radius of curvature is decreased [23, 24]. The tribological design of the cam-follower interface based on film thickness analysis is the key to reducing wear and friction losses [25, 26, 27]. Therefore, the value of maximum Hertzian stress is an important parameter for designers, however, the successful design of the cam and follower interfaces is related to many various parameters such as the lubricant film thickness.

5. Conclusion

In this study, numerical results on the subsurface stress field in Hertzian contacts under pure sliding conditions with consideration of the effect of sliding speed and coefficient of friction were presented. It was demonstrated from the results that low pure sliding velocities substantially change the magnitude and distribution of subsurface stresses due to the emergence of intense traction force in a pure sliding motion. In general, pure sliding causes the maximum von Mises stress to migrate towards the surface and this effect increases with increasing the coefficient of friction in contact. The coefficient of friction has a reduced effect on the value of subsurface stress along z-z axis compared to the effect of sliding speed. On the other hand, the coefficient of friction has a larger effect on shifting the region of maximum subsurface stress compared to the effect of sliding speed. On the basis of the maximum subsurface stress in the Hertzian contact of the cam-follower interface, the spherical-faced follower was subjected to more severe fatigue loading conditions compared to flat-faced follower. However, a comprehensive analysis of lubrication conditions as well as Hertzian stress is required for the successful design of concentrated contacts such as the cam-follower interface.

Conflict of Interest

The author declared no potential conflicts of interest with respect to the research, authorship, and publication of this article.

Funding

The author received no financial support for the research, authorship, and publication of this article.

References

- [1] Hertz, H., On the contact of elastic solids, *Z. Reine Angew. Mathematik*, 92, 1881, 156-171.
- [2] Sackfield, A., Hills, D.A., Some Useful Results in the Classical Hertz Contact Problem, *The Journal of Strain Analysis for Engineering Design*, 18, 1983, 101-105.
- [3] Johnson, K. L., *Contact Mechanics*, Cambridge University, Cambridge, 1987.
- [4] Sadeghi, F., Jalalahmadi, B., Slack, T.S., Raje, N., Arakere, N. K., A review of rolling contact fatigue, *Journal of Tribology*, 131(4), 2009, 041403.
- [5] Hamilton, G. M., Goodman, L. E., The stress field created by a circular sliding contact, *Journal of Applied Mechanics*, 33(2), 1966, 371-376.
- [6] Bryant, M.D., Keer, L.M., Rough contact between elastically and geometrically identical curved bodies, *Journal of Applied Mechanics*, 49(2), 1982, 345-352.
- [7] Chen, W. T., Stresses in some anisotropic materials due to indentation and sliding, *International Journal of Solids and Structures*, 5(3), 1969, 191-214.
- [8] Zhou, R.S., Cheng, H.S., Mura, T., Micropitting in rolling and sliding contact under mixed lubrication, *Journal of Tribology*, 111(4), 1989, 605-613.
- [9] Chen, W. W., Wang, Q. J., Thermomechanical analysis of elastoplastic bodies in a sliding spherical contact and the effects of sliding speed, heat partition, and thermal softening, *Journal of Tribology*, 130(4), 2008, 041402.
- [10] Chen, W. W., Wang, Q.J., Kim, W., Transient thermomechanical analysis of sliding electrical contacts of elastoplastic bodies, thermal softening, and melting inception, *Journal of Tribology*, 131(2), 2009, 021406.
- [11] Lee, S.C., Ren, N., The subsurface stress field created by three-dimensionally rough bodies in contact with traction, *Tribology Transactions*, 37(3), 1994, 615-621.
- [12] Bailey, D. M., Sayles, R. S., Effect of roughness and sliding friction on contact stresses, *Journal of Tribology*, 113(4), 1991, 729-738.
- [13] Zhang, H., Wang, W., Zhang, S., & Zhao, Z., Modeling of elastic finite-length space rolling-sliding contact problem, *Tribology International*, 113, 2017, 224-237.
- [14] Zhao, J., Sadeghi, F., Nixon, H.M., A finite element analysis of surface pocket effects in Hertzian line



contact, *Journal of Tribology*, 122(1), 2000, 47-54.

[15] Ali, Fadi, et al., Experimental and numerical investigation on the behavior of transverse limited micro-grooves in EHL point contacts, *Tribology International*, 84, 2015, 81-89.

[16] Ali, F., Křupka, I., Hartl, M., Reducing the friction of lubricated nonconformal point contacts by transverse shallow micro-grooves, *Proceedings of the Institution of Mechanical Engineers, Part J: Journal of Engineering Tribology*, 229(4), 2015, 420-428.

[17] Boucly, V., NÁŠlias, D., Green, I., Modeling of the rolling and sliding contact between two asperities, *Journal of Tribology*, 129(2), 2007, 235-245.

[18] Kogut, L., Etsion, I., A semi-analytical solution for the sliding inception of a spherical contact, *Journal of Tribology*, 125(3), 2003, 499-506.

[19] Faulkner, A., Arnell, R. D., The development of a finite element model to simulate the sliding interaction between two, three-dimensional, elastoplastic, hemispherical asperities, *Wear*, 242(1-2), 2000, 114-122.

[20] Nosonovsky, M., Adams, G.G., Steady-state frictional sliding of two elastic bodies with a wavy contact interface, *Journal of Tribology*, 122(3), 2000, 490-495.

[21] Tripp, H., Hertzian contact in two and three dimensions, NASA Technical Paper, 2473, 1985.

[22] Ball, A.D., Dowson, D., Taylor C.M., Cam and follower design, *Tribology Series*, Elsevier, 14, 1989, 111-130.

[23] Ball, A.D., *A Tribological Study of the Design and Performance of Automotive Cam*, Ph.D. Thesis, Department of Mechanical Engineering, University of Leeds, Leeds, UK, 1988.

[24] Muller, R., The effect of lubrication on cam and tappet performance, *MTZ*, 27, 1966, 58.

[25] Dyson, A., Kinematics and Wear Patterns of Cam and Follower Automotive Valve Gear, *Tribology International*, 13(3), 1980, 121-132

[26] Jamali, H.U., Al-Hamood, A., Abdullah, O.I., Senatore, A., Schlattmann, J., Lubrication Analyses of Cam and Flat-Faced Follower, *Lubricants*, 7(4), 2019, 31.

[27] Taylor, C.M., Fluid film lubrication in automobile valve trains, *Proceedings of the Institution of Mechanical Engineers, Part J: Journal of Engineering Tribology*, 208(4), 1994, 221-234.

ORCID iD

Fadi Ali  <https://orcid.org/0000-0001-5659-5259>



© 2020 by the authors. Licensee SCU, Ahvaz, Iran. This article is an open access article distributed under the terms and conditions of the Creative Commons Attribution-NonCommercial 4.0 International (CC BY-NC 4.0 license) (<http://creativecommons.org/licenses/by-nc/4.0/>).

How to cite this article: Ali F. Numerical Study on Subsurface Stress in Hertzian Contacts under Pure Sliding Conditions, *J. Appl. Comput. Mech.*, 6(SI), 2020, 1098–1106. <https://doi.org/10.22055/JACM.2019.31511.1882>

